NH$_3$-promoted hydrolysis of NO$_2$ induces explosive growth in HONO

Wanyun Xu[1], Ye Kuang[2,*], Chunsheng Zhao[3], Jiangchuan Tao[2], Gang Zhao[3], Yuxuan Bian[4], Wen Yang[5], Yingli Yu[3], Chuanyang Shen[3], Linlin Liang[1], Gen Zhang[1], Weili Lin[6], Xiaobin Xu[1]

[1] State Key Laboratory of Severe Weather, Key Laboratory for Atmospheric Chemistry, Institute of Atmospheric Composition, Chinese Academy of Meteorological Sciences, Beijing, 100081, China.

2 Institute for Environmental and Climate Research, Jinan University, Guangzhou, China.

[3] Department of Atmospheric and Oceanic Sciences, School of Physics, Peking University, Beijing, China

[4] State Key Laboratory of Severe Weather, Chinese Academy of Meteorological Sciences, Beijing, 100081, China

[5] State Key Laboratory of Environmental Criteria and Risk Assessment, Chinese Research Academy of Environmental Sciences, Beijing, 100081, China

[6] College of Life and Environmental Sciences, Minzu University of China, Beijing, 100081, China

Corresponding author: Ye Kuang (kuangye@jnu.edu.cn)

Abstract

The study of atmospheric nitrous acid (HONO), which is the primary source of OH radicals, is crucial to atmospheric photochemistry and heterogeneous chemical processes. The heterogeneous NO$_2$ chemistry under haze conditions was pointed out to be one of the missing sources of HONO on the North China Plain, producing sulfate and nitrate in the process. However, controversy exists between various proposed mechanisms, mainly debating on whether SO$_2$ directly takes part in the HONO production process and what roles NH$_3$ and the pH value play in it. In this paper, never before seen explosive HONO production (maximum rate: 16 ppb h^{-1}) was reported and evidence was found for the first time in field measurements during fog episodes (usually with 4<pH<6) and haze episodes under high relative humidity (pH≈4), that NH$_3$ was the key factor that promoted the hydrolysis of NO$_2$, leading to explosive growth of HONO and nitrate under both high and lower pH conditions. The results also suggest that SO$_2$ takes minor or insignificant part in the HONO formation during fog and haze events, but was indirectly oxidized upon the photolysis of HONO through subsequent radical mechanisms. Aerosol hygroscopicity significantly increased with the rapid inorganic secondary aerosol formation further promoting the HONO production as a positive feedback. For future photochemical and aerosol pollution abatement, it is crucial to introduce

34 effective NH_3 emission control measures, since the NH_3-promoted NO_2 hydrolysis is a large

35 daytime HONO source, releasing large amounts of OH radicals upon photolysis, which will

36 contribute largely to both atmospheric photochemistry and secondary aerosol formation.

37

1 Introduction

39   Nitrous acid (HONO) plays a vital role in atmospheric chemistry due to the fact that its

40 photolysis is a major source (Michoud et al., 2014;Kleffmann et al., 2005) of hydroxyl radical (OH)

41 which determines the atmospheric oxidative capacity and plays crucial role in tropospheric

42 chemistry in processes such as the ozone formation, the degradation of volatile organic compounds

43 and the secondary aerosol formation (Cheng et al., 2016;Wang et al., 2016). Hence, the source

44 study of nitrous acid (HONO) is of crucial importance for the understanding of the tropospheric

45 chemistry, for chemistry and climate modelling and for developing effective pollution control

46 strategies (Lu et al., 2018).

47   The North China Plain (NCP) is troubled by the persistent complex air pollution with high

48 loadings of both photochemical pollutants and particulate pollution (Zheng et al., 2015;Ran et al.,

49 2011) and the simultaneous mitigation of the two types of pollution has encountered trouble due

50 to the nonlinear dependence of ozone on NOx (Xing et al., 2018). Unknown daytime sources of

51 HONO caught attention during the past few years (Michoud et al., 2014;Liu et al., 2014;Su et al.,

52 2011) and results from a recent study indicate that an additional missing source is required to

53 explain more than 50% of observed HONO concentration in the daytime in Western China (Huang

54 et al., 2017). Results from several recent studies demonstrate that intense heterogeneous

55 conversion of NO_2 to HONO on particle surfaces might be a significant source of HONO (Liu et

56 al., 2014;Cui et al., 2018).

57   Two main HONO heterogeneous production pathways involving aerosol water and NO_2

58 were proposed. In light of drastic decrease of solar radiation during severe haze events and rich

59 ammonia conditions on the NCP, the first pathway hypothesized that NO_2 (g) dissolved in aerosol

60 water at aerosol pH > 5.5 rapidly formed HONO while oxidizing HSO_3^- (aq) to sulfate. The

61 stoichiometry of this mechanism is as follows (Cheng et al., 2016;Wang et al., 2016):

62    $2NO_2$ (aq) + HSO_3^- (aq) + H_2O (l) ➔ $2H^+$ + HSO_4^- (aq) + $2NO_2^-$ (aq).   (R1)
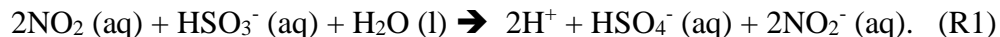
Based on this mechanism, good agreement between modelled and observed sulfate formation rates were achieved. However, the assumption that the pH of ambient aerosols can reach beyond 5.5 is a debatable issue. Results from several most recent studies indicate that the pH of ambient aerosols fall in the range of 3-5 in most cases (Ding et al., 2018;Liu et al., 2017a;Song et al., 2018). Given this, it was proposed that HONO and NO_2^- were produced in the hydrolysis process of NO_2, releasing OH radicals upon photolysis, which indirectly oxidize SO_2 to sulfate (Li et al., 2018b):

$$2NO_2\ (g) + H_2O\ (l) \rightarrow H^+ + NO_3^-\ (aq) + HONO. \quad (R2)$$
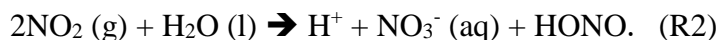
Results of Yabushita et al. (2009) suggest that anions (such as Cl^-, Br^- and I^-) greatly enhance the hydrolysis of NO_2 on water, and the NO_2 uptake coefficients of R2 can be enhanced several orders of magnitude by increasing electrolyte concentration. The ambient aerosol particles in the boundary layer are in aqueous phase under high RH (Liu et al., 2017b) and the aerosol or fog water is not pure with different dissolved anions (Wu et al., 2018;Lu et al., 2010). Therefore, HONO and nitrate formed through this mechanism should be independent of aerosol acidity, and should be primarily affected by the aerosol surface area density, aerosol liquid water content and NO_2 concentration (Li et al., 2018b). Moreover, recent theoretical simulations have proposed a HONO formation mechanism involving NO_2 and water and have identified that NH_3 can promote the hydrolysis of NO_2 (Li et al., 2018a) (R2). Despite of this, no direct evidence from field observations were available in this paper to support their findings.

Although the proposed HONO formation mechanisms are all heterogeneous reactions of NO_2, the details of how SO_2, pH and NH_3 are involved in heterogeneous formation are still under debate (Li et al., 2018b) and a clear mechanism is still missing in current models to explain both the daytime concentration of observed HONO and the secondary inorganic aerosol formation. Measurements of HONO are rare and simultaneous observations of HONO and aerosol physical and chemical characteristics are lacking to thoroughly analyze or directly support the aerosol heterogeneous HONO formation mechanisms involving NO_2. In this paper, we present for the first time simultaneous measurements of HONO, sulfate and nitrate as well as other precursor gases, oxidants and meteorological parameters during both fog and haze episodes under high ambient RH. Fog water pH is usually greater than 5.5 in eastern China (Safai et al., 2008;Lu et al., 2010), while calculations in this work and previous studies collectively indicate a moderately acidic

93   condition (4<pH<5) for fine particles in northern China winter haze. The observational results

94   unveil that NH_3 is the key factor that promotes the hydrolysis of NO_2, resulting in explosive

95   formation of HONO, nitrate and sulfate.

2 Site description and instruments

97   From 15th Oct. to 25th Nov. 2016, a field campaign intended to study sulfate formation was

98   conducted at the Ecological and Agricultural Meteorology Station ($39°09'N, 115°44'E$) of the

99   Chinese Academy of Meteorological Sciences. The site is partly composed of experimental

100   farmland and is also surrounded by farmland and small residential towns (nearest town ~1.5 km).

101   It is located between Beijing (~ 100km) and Baoding (~40km), two megacities on the North China

102   Plain (Fig. 1). During this field campaign, an In situ Gas and Aerosol Compositions Monitor

103   (IGAC, Fortelice International Co.,Taiwan) was used for monitoring water-soluble ions (Na^+, K^+,

104   Ca^{2+}, Mg^{2+}, NH_4^+, SO_4^{2-}, NO_3^-, NO_2^-, Cl^-) of $PM_{2.5}$ (particulate matter with aerodynamic diameter

105   less than 2.5 µm) and trace gases including HONO, SO_2, NH_3, HCl, and HNO_3 with a time

106   resolution of 1h. The IGAC system draws in ambient air through a PM10 inlet and passes the

107   sample through a sharp-cut PM2.5 cyclone at a flowrate of 16.7 L min^{-1}. The total length of the

108   stainless steel sampling line is approximately 2 m, with an inner diameter of 3.18 cm (1.25 inch),

109   resulting in a residence time below 6 s, suggesting that underestimates in NH_3 possibly caused by

110   adsorption on the stainless steel sampling tube as was proposed by Young et al. (2016) might be

111   unimportant. A vertical annular denuder wetted with dilute H_2O_2 solution (5x10^{-3} M) collects the

112   trace gases and converts SO_2 rapidly to SO_4^{2-}, preventing SO_2 from reacting with NO_2 in the

113   absorption solution to produce HONO artefacts. A scrub and impact aerosol collector under the

114   denuder is mounted at an inclined angle to capture particles based on impaction after condensation

115   growth. Two separate Ion Chromatographs are used to respectively analyze anions and cations for

116   the gas and aerosol liquid extracts which were injected from the denuder and the aerosol collector

117   once an hour. The detection limits are below 0.12 µg m^{-3} and the background concentration of

118   most water-soluble inorganic ions within the instrument were below 0.11 µg m^{-3}, only with SO_4^{2-}

119   showing a background concentration of 1.10 µg m^{-3} (Young et al., 2016). Considering the severe

120   pollution state the NCP is under, these measurement uncertainties are fully acceptable. The

121   instrument has shown good performance in the past, agreeing well with filter based samples (Liu

122   et al., 2017a). Standard LiBr solution was continuously added to the aerosol liquid extracts during

123 the measurements, to ensure the sampling and analyzing process is stable. The swing amplitude

124 was within the range of three standard deviation, confirming the stability of the ion analyzing

125 system throughout the campaign. A mixed standard solution was diluted to perform multipoint

126 calibrations (at 5, 10, 20, 50, 100, 200, 500 and 1000 ppb concentrations) at the beginning and at

127 the end of the campaign for the ions Na^+, K^+, Ca^{2+}, Mg^{2+}, NH_4^+, Li^+, SO_4^{2-}, NO_3^-, NO_2^-, Cl^-, Br^-,

128 with the R^2 of the calibrations reaching above 0.9999. A comparison between NH_3 observed by

129 IGAC and by an economical NH_3 analyser (LGR, DLT-100, details see Meng et al. (2018)) yielded

130 an overall slope of 0.91 with R=0.63 (Fig.S1a). A better comparison result (slope of 1.03, R=0.74)

131 would be obtained if data associated with RH≥80 were excluded (Fig.S1b). The overestimation of

132 LGR instruments compared to denuder based instruments has also been reported in Teng et al.

133 (2017), suggesting possible interference of water vapor on NH_3 measurements. As can be seen in

134 Fig.S2, both instruments captured the same the diurnal variation of NH_3 during the four case

135 episodes in this study, which proves that the IGAC instrument was able to capture the overall

136 variation trends of NH_3. Since both instruments have their uncertainties, we decided to use the

137 NH_3 measured by the IGAC instrument for better consistency with the other data.

138 NOx and CO were observed using commercial instruments from Thermo Electronics

139 (Model 42CTL and 48CTL), while the Aerolaser AL2021 H_2O_2-monitor was used to measure

140 H_2O_2 concentrations. The ambient RH, temperature, wind speed and wind direction were observed

141 using an automatic weather station. The dry state particle number size distributions (PNSDs) in

142 the diameter range of 3nm to 10μm, were jointly measured by a scanning mobility particle size

143 spectrometer (SMPS) and an Aerodynamic Particle Sizer (APS, TSI Inc., Model 3321). The

144 ambient aerosol liquid water concentrations were calculated based on measurements of a three-

145 wavelength humidified nephelometer system (Kuang et al., 2018). The aerosol hygroscopicity

146 parameter κ (Petters and Kreidenweis, 2007) is calculated using the method proposed by Kuang et

147 al. (2017).

3 Observed simultaneous rapid increase of HONO, nitrate and sulfate

149 The time series of HONO, sulfate, nitrate and ammonium and precursor gases,

150 meteorological parameters and other parameters are shown in Fig. 2. During this observation

151 period, HONO concentration ranged from 0.31 to 17.6 ppb (ranged from 0.3 to 6.0 ppb during

152 most periods) with an average of 3.0 ppb. The $HONO/NO_2$ ratio ranged from 0.03 to 0.75 with an

153 average of 0.18, which is higher than the average $HONO/NO_2$ ratio previously observed in China

154 (Liu et al., 2014;Cui et al., 2018). NO_2 concentration ranged from 7.5 to 60.1 ppb with an average

155 of 32.0 ppb. NH_3 concentration ranged from 0.05 to 30 ppb with an average of 12.3 ppb. Four

156 rapid HONO formation events were identified in Fig.2, two under foggy conditions and the other

157 two under high RH conditions.

3.1 Explosive growth of HONO during fog episodes

159 Two dense fog episodes with rapid HONO increase were observed for the first time in

160 China, occurring on the 4th and 5th Nov. 2016. From satellite images (Fig. 1) it can be seen that on

161 the 5th Nov., a wide area of the NCP was shrouded by fog before noon (about 11:30) including the

162 observation site, however, the fog area reduced in the afternoon (about 13:30) and dissipated near

163 the observation site. The evolution of the fog-shrouded area during these two days was also

164 observed by a geostationary satellite (http://www.eorc.jaxa.jp/ptree/index.html). These two fog

165 episodes offer us a great opportunity to study the hydrolysis process of NO_2 (R2) and the role of

166 SO_2 in heterogeneous HONO production in fog water (R1), which usually show pH above 5.5

167 (Safai et al., 2008;Lu et al., 2010).

168 The time series of simultaneously observed meteorological parameters, concentrations of

169 nitrate, ammonium, sulfate and their precursor gases SO_2, NO_2, NO and NH_3, as well as

170 atmospheric oxidants such as O_3, H_2O_2 and other parameters including CO, which is indicative of

171 transport processes during the two days with fog episodes are shown in Fig. 3. From 0:00 (Beijing

172 local time) on the 4th Nov., the ambient RH continuously increased and reached 100% near 5:00,

173 and lasted about 8.5 hours before it dropped below 100% near 13:30. However, at 15:30, the

174 ambient RH began to rise again and reached 100% near 19:30, and then sustained until 12:00 on

175 the 5th Nov. The latter fog episode lasted about 18.5 hours.

176 During the first fog episode, the rapid increases of HONO, nitrate, sulfate and ammonium

177 were observed from 8:50 to 11:30 (Case1). HONO increased from 3.6 ppb to 10.6 ppb, with the

178 most rapid increase occurring around 11:00 at a rate of 5.5 ppb h^{-1}. During the HONO increasing

179 period, the variation characteristics of related trace gases and other parameters are as follows. NH_3

180 concentration increased slowly at first and then increased drastically near 11 am (10 ppb h^{-1}). SO_2

181 concentration remained almost constant at first and then increased from near 0.25 ppb to 0.4 ppb.

182 NO_2 concentration increased continuously with a small magnitude, while NO concentration

183 increased first and then decreased. H_2O_2 concentration is continuously increasing, but O_3
184 concentration remained near zero. CO concentration remained almost constant (~2.5 ppm),
185 suggesting that there was no evident plume transport during this process. Wind speed was less than
186 2 m s^{-1}, and dropped almost to 0 m s^{-1} when HONO concentration dramatically increased, further
187 supporting the fact that the drastic increase was not caused by transport processes. Ammonium,
188 nitrate and sulfate concentration steadily increased from 7.5, 13.2, 13.7 µg m^{-3} to 14.3, 30.4,
189 31.0 µg m^{-3}, respectively. A noticeable increase in nitrite was also observed, when HONO
190 increased most rapidly. It should be noted that the cutting diameter of the IGAC instrument is 2.5
191 µm, which means that observed concentrations only represent the variation of inorganics ions in
192 aerosol water, and that of fog droplets were not included.

193   During the second fog episode, HONO, nitrate, sulfate and ammonium started to increase
194 rapidly from 9:30 and reached a plateau near 12:30, when the fog started to dissipate (Case2).
195 HONO increased from 3 ppb to 9.5 ppb, with the fastest increase occurring near 11:00 at a rate of
196 3.5 ppb h^{-1}. Variation characteristics of other parameters are as follows. NH_3 concentration
197 increased steadily from 5 ppb to 24 ppb. SO_2 concentration increased steadily from 0.25 ppb to
198 1.25 ppb. NO_2 concentration remained almost constant at the very beginning (near 40 ppb) and
199 then increase slightly, while NO concentration remained almost constant (near 30 ppb) throughout
200 the entire fog period. H_2O_2 concentration increased slightly at first and then rose rapidly towards
201 the end of the fog period. O_3 concentration increased very slightly. CO concentration remained
202 also near constant (~3 ppm). Wind speed was steady and less than 2 m s^{-1} at the beginning, however,
203 began to increase quickly at noon. Ammonium, nitrate and sulfate concentration steadily grew
204 from 8.1, 17, 3.8 µg m^{-3} to 15.3, 39.3, 8.0 µg m^{-3}, respectively. The variation of nitrite was very
205 similar to that of HONO. The variation of wind speed demonstrate that at the very beginning of
206 the HONO increase, the air mass was relatively stagnant, but became windy when the fog
207 dissipated.

208 **3.2 Explosive growth of HONO during haze episodes with high RH conditions**

209   The two periods with rapid HONO increase under high RH conditions occurred on the 11th
210 and 14th Nov., respectively. The time series of simultaneously observed meteorological parameters,
211 concentrations of nitrate, ammonium, sulfate and their precursor gases SO_2, NO_2, NO and NH_3, as
212 well as oxidants including O_3, H_2O_2 and other parameters such as CO concentration, aerosol

volume concentration in dry state and aerosol liquid water content during the two days are shown in Fig.4.

On the 11th Nov., HONO started rising from 6:30 (3.4 ppb) and came to a halt at 9:00 (11.5 ppb) (Case 3). The quickest increase of HONO occurred near 9 o'clock with a rate of 5.6 ppb h^{-1}. The key features of other parameters are introduced in the following. The ambient RH decreased rapidly (from foggy condition to near 75%). NH_3 increased slowly at first and then grew rapidly. NO_2 increased slowly and SO_2 remained low. The total volume concentration of $PM_{2.5}$ was decreasing. Ammonium, nitrate and sulfate concentrations increased very slowly at first and then evident increase was observed in ammonium and nitrate. The decrease in dry state volume concentration of $PM_{2.5}$ demonstrate that the air mass is not quite steady due to transport or boundary layer processes. The slight increase of nitrate and sulfate despite the drop in total $PM_{2.5}$ concentration suggest that the nitrate and sulfate produced during the increasing process of HONO outgrew those lost to boundary layer mixing and transport.

On the 14th Nov., HONO increased drastically near 11:00, reaching 17.6 ppb at 11:30 (16.1 ppb h^{-1}) and then dropped promptly to 4 ppb at 12:30 (Case 4). This phenomenon took place when the fog dissipated and the ambient RH abruptly dropped to near 85%. Key variation features of other parameters are as follows. NH_3 increased rapidly from 9.7 ppb to 30 ppb. NO_2 concentration was increasing quickly, while SO_2 concentration remained low. The concentration of sulfate and nitrate also increased quickly. Volume concentration of $PM_{2.5}$ was decreasing, indicating that even more sulfate and nitrate were formed than the observed growth in their concentrations. The photolysis of HONO was high probably the cause for its drastic decrease. Note that the HONO was not increasing during the period where only NO_2 increased rapidly and NH_3 varied little.

4 Discussions

4.1 HONO budget analysis

In these four rapid HONO increasing episodes, the maximum HONO growth rates (d[HONO]/dt) all exceed 5 ppb h^{-}, and even reach beyond 16 ppb h^{-1}. Such high HONO growth rates as observed in this study were not yet reported in literature. In this section, we discuss whether these HONO formation events can be explained by current known mechanisms and which mechanisms are determining the variation of HONO.

242   The net HONO production rate can be estimated by accounting for all the currently known
243   sources and sinks using the following equation:

244   $$P_{HONO}^{net} = P_{emi} + P_{hom}^{net} + P_{het} - L_{pho} - L_{dep},$$ (Eq.1)

245   where P_{emi} is the total emission rate of HONO, P_{hom}^{net} the net HONO production in homogenous
246   gas phase reactions, P_{het} the HONO produced via heterogeneous reactions, L_{pho} the loss of HONO
247   due to photolysis and L_{dep} the loss of HONO due to deposition.

248   Previous studies have shown that HONO can be emitted through biomass burning and
249   vehicles (Nie et al., 2015;Huang et al., 2017). Biomass burning contributes to HONO mainly by
250   increasing particle surface area and NO_2 conversion efficiency (Nie et al., 2015). Under foggy
251   conditions, surface area was not the limiting factor to the NO_2 conversion. During the haze events,
252   particle surface area was decreasing due to decreasing humidity and aerosol water content. Hence,
253   the variation of surface area cannot explain the observed HONO increases. According to the
254   mapped fire spots on the days of the HONO events (Fig.S3), there was no fire within 20 km
255   distance to the site. K^+ is often used as an indicator for biomass burning. The average K^+
256   concentration during the whole campaign ranged from 0.022 to 5.95 μg m^{-3}, with an average of
257   1.28 μg m^{-3}. The K^+ level during the four events were 1.39, 1.08, 1.51 and 1.54 μg m^{-3}, respectively,
258   showing no evident sign of biomass burning. Hence, only vehicle emissions were considered in
259   this study.

260   Vehicle emissions can be estimated using the following equation:

261   $$P_{vehicle} = R_{emission} \times [NO_x]_{vehicle},$$ (Eq.2)

262   where $R_{emission}$ is the vehicle emission ratio and $[NO_x]_{vehicle}$ the NOx concentration from vehicle
263   emissions. The NO/NOx ratio during the HONO increasing episodes ranged from 0.37 to 0.76,
264   suggesting that the air masses were relatively aged compared to freshly emitted air mass from
265   exhaust (NO/NOx>0.9). Here, $P_{vehicle}$ is estimated assuming all the measured NOx came from
266   vehicle emissions and an emission ratio of 1%, which is higher than the upper limit of 0.8% used
267   in Huang et al. (2017), to obtain an upper limit for vehicle emissions.

268   HONO can be formed in gas phase reactions of NO with OH radicals and is lost through
269   direct reactions with OH radicals. The net production of HONO via homogeneous reactions can
270   be estimated using the equation:

271   $$P_{hom}^{net} = k_{NO+OH}[NO][OH] - k_{HONO+OH}[HONO][OH],$$ (Eq. 3)

where k_{NO+OH} (7.2×10^{-12} cm^{-3} s^{-1}) and $k_{HONO+OH}$ (5.0×10^{-12} cm^{-3} s^{-1}) are the rate constants of the reactions of NO and HONO with OH, at 298 k, respectively (Li et al., 2012). The diurnal variation of OH concentrations was inferred from Whalley et al. (2015), replacing OH under fog conditions with 1×10^5 cm^{-3}.

Heterogeneous conversion of NO$_2$ on aerosol and ground surface is considered a major source for HONO. However, the detailed mechanism (R1 or R2?) is still under debate and different studies have shown a large variability in the range of estimated NO$_2$ uptake coefficient. Typically, the conversion of NO$_2$ on aerosol and ground surface is parameterized as a linear function of NO$_2$ uptake coefficients and surface to volume ratios (surface area densities) (Xue et al., 2014;Li et al., 2018b):

$$P_{het} = (k_g + k_a)[NO_2], \tag{Eq.4-1}$$

$$k_g = \frac{1}{8} \cdot \vartheta_{NO2} \cdot \gamma_g \cdot \frac{S}{V}, \tag{Eq.4-2}$$

$$k_a = \frac{1}{4} \cdot \vartheta_{NO2} \cdot \gamma_a \cdot S_a, \tag{Eq.4-3}$$

where ϑ_{NO2} stands for the mean molecular speed, γ_g and γ_a for the uptake coefficient on ground and aerosol surface, S/V for the surface to volume ratio and S$_a$ for the ambient aerosol surface area density. For NO$_2$ conversion on ground surface, γ_g is assumed to be 1×10^{-6} during nighttime and 2×10^{-5} during daytime and S/V is assumed to be 0.1 m^{-1} as in Vogel et al. (2003). Since no measurements of fog droplet surface areas were made in this experiment, we use a γ_a range of 1×10^{-4} to 1×10^{-3} as suggested by Li et al. (2018b) and a wide range of surface area densities to account for both aerosol and fog conditions. Additionally, for non-fog conditions, the ambient aerosol surface area density calculated using the simultaneously measured PNSD and aerosol hygroscopicity parameter derived from measurements of a humidified nephelometer system and $\gamma_a = 1 \times 10^{-4}$ is applied to further calculate the variation of the HONO production on aerosol surface.

HONO loss through photolysis reactions were calculated as:

$$L_{pho} = J_{HONO}[HONO], \tag{Eq.5}$$

where JHONO was modelled using the TUV radiative transfer model (version 5.3, http://www2.acom.ucar.edu/modeling/tuv). The required single scattering albedo and aerosol angstrom exponent were estimated using simultaneously measured PNSD and BC measurements (Kuang et al., 2015), while the 550nm aerosol optical depth (AOD) was assumed to vary with RH (Table S1).

302   Loss through dry deposition was estimated using equation 6:

303      $L_{dep} = \frac{v_{dep}}{H}[HONO],$ (Eq.6)

304 where the dry deposition rate v_{dep} was assumed to be 0.3 cm s^{-1} according to (Stutz et al., 2002)

305 and the boundary layer height H was interpolated from ECWMF ERA-interim data

306 (http://apps.ecmwf.int/datasets/data/interim-full-daily/).

307   The comparison between the calculated HONO net production rate and actually measured

308 HONO variation rate (d[HONO]/dt) is displayed in Fig. 5. The estimated upper limit for vehicle

309 emissions displays little variability during the day, with slight decreasing trends during the four

310 events, proving that the observed HONO production could not have been caused by direct vehicle

311 emissions. The net gaseous phase production of HONO (P_{hom}^{net}) contributed 0.15-0.18, 0.04-0.07,

312 0.27-1.04 and 0.25-1.53 ppb h^{-1} during the 4 case events, displaying little influence during fog

313 events and more during haze events. However, the estimated P_{hom}^{net} was far from sufficient to

314 explain the observed d[HONO]/dt. Dry deposition was typically high during the night within the

315 shallow nocturnal boundary layer and decreased during the day with the increase of the boundary

316 layer height. The calculated L_{dep} contributed 0.5-0.9, 0.4-0.6, 2.7-4.3 and 0.05-0.3 ppb h^{-1} to the

317 loss of HONO. No significant decreases in L_{dep} were observed during the two fog events, while

318 increases were detected during the cases on 11th and 14th Nov. Not only was the variation in L_{dep}

319 unable to explain observed HONO productions, it further added to the discrepancy between

320 observed and calculated d[HONO]/dt. During the four case events the J_{HONO} respectively increased

321 from 0.7×10^{-4} to 2.5×10^{-4} s^{-1}, 1.6×10^{-4} to 2.4×10^{-4} s^{-1}, 0.03×10^{-4} to 1.4×10^{-4} s^{-1} and 1.6×10^{-4} to

322 4.4×10^{-4} s^{-1}, with L_{pho} contributing 0.9-8.9, 2.2-7.8, 0.03-5.5 and 0.8-26.4 ppb h^{-1} to the loss of

323 HONO. J_{HONO} increased significantly by the end of the HONO growth events to 2.9×10^{-4}, 4.3×10^{-4}

324 ^{4}, 2.6×10^{-4} and 6.6×10^{-4} s^{-1}, respectively, suggesting that the rapid drop of HONO concentrations

325 was high probably caused by the rapid photolysis. Overall, L_{pho} contributed most to the discrepancy

326 between observed and calculated d[HONO]/dt.

327   Generally, the observed and calculated d[HONO]/dt agreed better with each other outside

328 the HONO explosive growth periods, showing overestimations when aerosol liquid water contents

329 were high, suggesting possible overestimation in the NO$_2$ uptake coefficient in the

330 parameterization of P_{het}. This further suggests that the observed discrepancies in HONO

331 production have mainly been caused by uncertainties in the heterogeneous formation estimates.

332 The fact that HONO drastically increased while NO$_2$ varied little (9:30 to 11:30, 5th Nov. and 6:30

to 8:30, 11th Nov.) or hardly increased even under drastic increases of NO_2 (8:30 to 11:30, 14th

Nov.), but displayed explosive growth with increasing NH_3, could not be explained by current

known HONO sources (direct emission or gas phase reactions). Additionally, these rapid

increasing HONO phenomena were all observed under foggy or high RH conditions, which further

affirms the suspicion that the HONO increase was caused by heterogeneous conversion of NO_2.

4.2 Heterogeneous HONO formation mechanism

As manifested in Sect. 4.1, the unknown HONO source and the overestimates in HONO

production were both linked to our limited understanding on the heterogeneous HONO formation

mechanism. In this section, we try to evaluate the relative contribution of the currently known

heterogeneous HONO formation pathways (R1 and R2) and reveal the reason for their limitations

in explaining the observed HONO growth.

To evaluate which process (R1 or R2) was dominating the heterogeneous production of

HONO, we assume that HONO was produced in aerosol and fog water simultaneously via R1 and

R2. Since measurements of fog liquid water content or fog droplet surface area density were not

made, we cannot directly quantify the absolute HONO production in fog. However, we can make

a few assumptions to compare the relatively HONO contribution via R1 and R2. First, it was

assumed that the observed sulfate production (d[SVI]/dt) was caused by the reaction of SO_2 with

H_2O_2, O_3, NO_2, transition metal ions (TMI: Fe^{3+} and Mn^{2+}). Calculations were performed

according to Cheng et al. (2016), using the same pH dependent TMI concentrations and the

actually measured SO_2, H_2O_2, O_3 and NO_2 concentrations (Table S2). For the two fog episodes on

4th and 5th Nov. 2016, the mean diameter of fog droplets was assumed to be 7.0 μm and the liquid

water content was assumed to be 0.3 g m^{-3} according to Shen et al. (2018). For the haze episodes

on the 11th and 14th Nov. 2016, the mean aerosol diameter under ambient conditions was estimated

to be 0.65-1.22 and 0.9 μm, while the liquid water content was calculated to decrease from 3.4×10^{-4}

to 7.8×10^{-5} g m^{-3} on the 11th Nov and assumed to be 0.01 g m^{-3} on the 14th Nov. during the

transition from fog to haze. The sulfate production rate and relative contribution of each oxidation

pathway to the total sulfate production rate was obtained and depicted in Fig.6. For the two fog

episodes, assuming pH=6, the estimated average sulfate production rates are 11.7 and 31.6 μg m^{-3} h^{-1}

approximately 4 times of that observed within $PM_{2.5}$, which might be an underestimation,

considering the liquid water content of fog droplets are at least a magnitude higher than that of

aerosols. For the two haze episodes, using the pH values estimated using ISORROPIA (forward

364 mode and metastable assumption (Song et al., 2018)), the estimated average sulfate production

365 rates are 0.06 and 1.8 μg m^{-3} h^{-1}, about 10% of that observed within PM$_{2.5}$. Following the

366 calculations of Cheng et al. (2016), we have considered the influence of ionic strength on the

367 reaction rates and set constraints on the maximum ionic strength (I_{max}), which might have caused

368 underestimations for all reaction routes, since the calculated ionic strength commonly exceeded

369 I_{max}. Underestimated transition metal ion concentrations may also be partly responsible for the

370 underpredicted sulfate production, since the TMI catalysis route has recently be pointed out to be

371 the dominant SO$_2$ heterogeneous oxidation pathway {Shao, 2019 #2155}. Additionally, there also

372 might be other neglected SO$_2$ oxidation pathways, which will lead to overestimates in the sulfate

373 fraction produced by the NO$_2$ oxidation pathway. Therefore, we can only yield an upper limit for

374 the HONO production rate of R1:

375 $$\frac{d[HONO]}{dt}_{R1} = 2 \times frac_{SO_2+NO_2} \times \frac{d[SVI]}{dt}_{obs}, \hspace{2cm} \text{(Eq.7)}$$

376 where $frac_{SO_2+NO_2}$ is the contribution fraction of the NO$_2$ oxidation pathway to the total sulfate

377 production. Note that the calculated HONO production rate can only represent the production

378 within PM$_{2.5}$.

379 By further assuming that all the observed nitrate production (d[NO$_3^-$]/dt) was caused by reaction

380 R2 and by the reaction of NO$_2$ with OH radicals (k_{NO_2+OH}=3.2×10^{-12} cm^3 s^{-1}), the HONO

381 production rate of R2 would be:

382 $$\frac{d[HONO]}{dt}_{R2} = \frac{d[NO_3^-]}{dt}_{obs} - k_{NO_2+OH}[NO_2][OH]. \hspace{2cm} \text{(Eq.8)}$$

383 The contribution fraction of the two reactions to the heterogeneous HONO production in aerosol

384 and fog liquid water content can be calculated by:

385 $$f_{R1} = \frac{d[HONO]}{dt}_{R1} / \frac{d[HONO]}{dt}_{R1+R2} \quad \text{and} \hspace{2cm} \text{(Eq.9-1)}$$

386 $$f_{R2} = \frac{d[HONO]}{dt}_{R2} / \frac{d[HONO]}{dt}_{R1+R2}. \hspace{2cm} \text{(Eq.9-2)}$$

387 Assuming the pH of fog droplets falls within the range of 4 to 6, f_{R2} was estimated to range

388 from range from 75.5 to 99.5% and from 81.2 to 99.5% during the 4th and 5th Nov. 2016,

389   respectively. For the two haze events on 11th and 14th Nov., the f_{R2} corresponding to the pH values

390   modelled by ISORROPIA would be 98.2% and 97.3%.

391   These results suggest that, reaction R2 is the dominant contributor to the heterogeneous

392   HONO production, while R1 is more important under high pH conditions. Under the assumed

393   upper limit of pH, R1 can contribute up to 24.5%, 18.8% to the observed HONO growth during

394   the fog events. This is in accordance with results from Wang et al. (2016) and Cheng et al. (2016),

395   which suggested that R1 was more likely to happen during fog episodes or under NH_3 neutralized

396   conditions (3,4). For the two haze events, R1 contributed very little (1.8% and 2.7%) to the

397   observed HONO growth.

398   Since R2 seems to be the dominant contributor to the observed HONO production, it is

399   important to evaluate whether the parameterizations in current literature can accurately describe

400   the HONO production process of R2. The HONO production rate of R2 is typically parameterized

401   as in Eq.4, where the NO_2 concentration and the surface area density of fog droplets/aerosol

402   particles are the controlling factors of the NO_2 uptake, as opposed to the pH of the water droplets

403   (Li et al., 2018b;Yabushita et al., 2009). Based on the reactive uptake coefficient of NO_2 (γ_{NO_2}) in

404   Yabushita et al. (2009) and Li et al. (2018b), we have calculated the HONO production rate of R2

405   under different conditions (Fig.S4). During foggy conditions, the HONO production rate should

406   be higher than 1 ppb (ppb $NO_2 \cdot h)^{-1}$. The NO_2 concentration during the two fog episodes ranged

407   between 40 to 50 ppb, therefore, the HONO production rate would have been higher than 40 ppb h^{-1}

408   ^{1}. However, no rapid increase of HONO was observed unless NH_3 was simultaneously increasing.

409   As already mentioned before, under hazy conditions, P_{het} significantly overestimated the HONO

410   production when relative humidity was high and large ambient aerosol surface area densities were

411   observed (Fig5), while it failed to reproduce the growth in HONO on the morning of the 11th Nov.

412   2016. These results indicate that R2 is missing the important impact of NH_3 in the heterogeneous

413   HONO production and that the γ_{NO_2} range is at least overestimated when NH_3 is not abundant

414   enough.

415   Recent theoretical simulation results ascertain that NH_3 can promote the hydrolysis of NO_2

416   and contribute to HONO formation via R2 (Li et al., 2018a). This conclusion is consistent with the

417   observed phenomena that HONO only increased rapidly when NH_3 was simultaneously increasing.

418   Considering the influence of NH_3 and sulfate on the aerosol pH, under our observed NH_3

419   concentration range, NH_3 has negligible impact on pH values (Guo et al., 2017), especially under

420 high RH conditions. This further proves that the NH_3-promoted hydrolysis of NO_2 is independent

421 of the pH value. Another phenomenon worth noting is that, in Case 3, HONO was increasing

422 rapidly even under the drastic decrease in ambient RH, which demonstrates that the impact of NH_3

423 on HONO formation should be even more important than that of aerosol liquid water content.

424 However, the hydrolysis of NO_2 needs water to be involved, thus, the importance of water content

425 under different conditions remains to be elucidated.

426   To further investigate the acceleration effect of NH_3 on the hydrolysis of NO_2, we have

427 examined the correlations between the NO_2-to-HONO (HONO/NO_2 ratio), NO_2-to-NO_3^- (NO_3^-

428 /NO_2 ratio) conversion efficiencies and the NH_3 concentration during the entire field campaign

429 (Fig.7). Note that only data points during nighttime (18 pm to 6 am) and with ambient RH higher

430 than 80% are displayed in Fig.7. Daytime data were excluded, because HONO would quickly

431 photolyze as soon as sunlight was available. Even if there was rapid HONO production, the

432 corresponding increase of HONO might not be observable due to its quick photolysis. The reason

433 for only including data with ambient RH higher than 80% is that the quick hydrolysis of NO_2

434 requires water to be involved. However, the overall hygroscopicity of ambient aerosols during this

435 field campaign was relatively low, with an average hygroscopicity parameter κ of 0.14, and the

436 volume contribution of liquid water to the total volume concentrations of ambient aerosols was

437 quite low when ambient RH is below 80% (Kuang et al., 2018). The correlation coefficient between

438 HONO/NO_2 ratio and the NH_3 concentration reaches 0.68, while that between NO_3^-/NO_2 ratio and

439 NH_3 concentration only reaches 0.48, since the source of NO_3^- is much more complicated than that

440 of HONO. These results have further verified that NH_3 promotes the NO_2 hydrolysis and HONO

441 production. The correlation of HONO/NO_2 to NH_3 is highly nonlinear, HONO/NO_2 increases

442 rapidly with NH_3 when NH_3 reaches above 10 ppb.

443

444 **4.3 Feedback between HONO formation and inorganic secondary aerosol formation**

445   According to the discussions in Sect.4.2, NH_3 promotes the hydrolysis of NO_2, producing

446 nitrate and most of the observed HONO. However, the connection between the NH_3 promoted

447 hydrolysis and the simultaneous rapid sulfate production remains unexplained. As was already

448 discussed in Sect.4.2, the sulfate production rate calculated based on currently known SO_2

449 oxidation pathways largely underestimates the observed sulfate growth, indicating that there might

450 be neglected oxidation pathways. Li et al. (2018b) pointed out that NO_2 can oxidize S(IV)

451 indirectly via free radical mechanism (the involved reactions RS1 to RS5 proposed in Li et al.
452 (2018b) listed in the supplement). The key step of the proposed S(IV) oxidation pathway is the
453 photolysis of HONO to produce OH radicals (RS1). OH can oxidize S(IV) to form bisulfate or
454 sulfate through reaction RS2 and produce HO_2. HO_2 can react with NO to produce NO_2, or react
455 with itself to produce H_2O_2. As was depicted in Fig.5, the radiation during the fog/haze events was
456 already strong enough to photolyze the produced HONO and release OH radicals at the same rates
457 as L_{pho} in Sect. 4.1, indicating there was strong OH production, especially near the end of the
458 events. For the two fog events, no AOD measurements were available. Assuming AOD=2.5 for
459 foggy conditions, the lifetime of HONO (only considering the photolysis process) were estimated
460 to decrease from 4.2 to 1.1 h, 1.7 to 1.1 h during the growth of HONO and to drop to 1.0 and 0.7 h
461 by the time of the drastic decreases in HONO. In the haze event on the 11th Nov., AOD
462 measurements were also not available due to cloud coverage, however, sensitivity study shows
463 that the calculated HONO lifetime are much more sensitive to the AOD as opposed to the COD
464 values (increasing 3.1 and 0.4 h per 0.1 increase in AOD and COD, Fig.S5). The HONO lifetime
465 dropped from 2.0 h (by the time of the HONO peak) to 1.1 h (by time of the HONO decrease).
466 During the case on the 14th Nov. 2016, the relative humidity decreased from 100% (10:00-11:00)
467 to 86% (11:30), suggesting that this was a fog dissipation process. The HONO lifetime was
468 estimated to be 1.7 h between 10:00 to 11:00, proving that the photolysis process was relatively
469 weaker during the rapid increase of HONO. The estimated HONO lifetime rapidly decreased to
470 0.6 h by 12:00, resulting in accelerated HONO dissociation and OH production. The increase in
471 H_2O_2 observed during and after the increase of HONO, might be an indirect evidence of the HO_2
472 production and occurrence of RS2. The observed H_2O_2 concentrations were much higher than the
473 assumptions of 0.01 ppb made in Cheng et al. (2016), which was also pointed out by Ye et al.
474 (2018). Under the assumed pH range for fog and the calculated pH range for aerosol, the estimated
475 sulfate production was dominated by the SO_2 oxidation via H_2O_2 (Fig.6). This indicates that both
476 the calculated and the yet unexplained sulfate production were linked to the photolysis of HONO.
477   NH_3 promoted the hydrolysis of NO_2, producing HONO and nitrate. HONO easily photolyzes
478 releasing OH radicals, which further converted to HO_2 and H_2O_2. The highly oxidative free radicals
479 and H_2O_2 collaboratively boosted the formation of sulfate. Hence, diurnal variations of NH_3 should
480 have exerted significant influences on the diurnal variations of HONO and inorganic aerosol
481 chemical components (sulfate, nitrate and ammonium, SNA). The average diurnal variations of

482 NO_2, NH_3, HONO as well as SO_2 concentrations during this field campaign are shown in Fig.8a.

483 The average HONO concentration during nighttime is higher than that during daytime due to the

484 quick photolysis of HONO upon solar irradiation. The NH_3 concentration begins to increase in the

485 morning (near 8:00 LT) the reaches a plateau in the afternoon (8.5 to 15.5 ppb in average), and the

486 SO_2 concentrations shows a similar diurnal variation to that of NH_3. This type of diurnal variation

487 of SO_2 was also found by Xu et al. (2014), however, the cause of the common diurnal pattern

488 between NH_3 and SO_2 during this field campaign requires further investigation. The NO_2

489 concentration increases quickly in the afternoon and decreases in the evening.

490   As shown in Fig.8b, the increase of NH_3 from morning to the afternoon was accompanied

491 with the increase of mass fractions of nitrate and sulfate in $PM_{2.5}$ (The mass fractions of different

492 aerosol chemical compositions were obtained by using the measured dry state PNSD to calculate

493 volume concentration of $PM_{2.5}$, assuming that the density of aerosols in dry state is 1.5 g cm^{-3} (Yin

494 et al., 2015). The results shown in Fig.8b indicate that the molecular concentration increase in

495 nitrate from the morning to the afternoon is much faster than that of sulfate, again supporting the

496 fact that the NH_3-promoted NO_2 hydrolysis, which only produces HONO and nitrate directly, was

497 the main contributor to the observed explosive HONO formation. The evident morning increase

498 of inorganic aerosol component fractions resulted in prominent increases of aerosol hygroscopicity,

499 displaying an average κ anomaly of +0.04 during noontime (Fig.8c). From the morning to the

500 afternoon, the ambient RH decreases quickly, however, the increase of aerosol hygroscopicity can

501 retard the decrease of aerosol liquid water content and surface area density of ambient aerosols.

502 This might acts as a positive feedback, further enhancing the hydrolysis of NO_2 as well as the

503 nitrate and sulfate formation.

504 **5. Summary and atmospheric implications**

505   Explosive HONO growth (observed maximum d[HONO]/dt=16.1 ppb h^{-1}) was observed

506 for the first time on the NCP during fog and haze episodes with high RH conditions, only occurring

507 with evident increases in NH_3, indicating that NH_3 is the key factor promoting the hydrolysis of

508 NO_2, resulting in rapid HONO and nitrate formation. NH_3 concentrations during the observation

509 period exhibit a distinct diurnal variation with an increase in the morning and a peak in the

510 afternoon (8.5 to 15.5 ppb in average). The increase of NH_3 promotes the hydrolysis of NO_2, giving

511 significant rise to HONO and nitrate concentrations. Produced HONO released OH radicals upon

512 photolysis, which further oxidized SO_2 to sulfate through gas phase and heterogeneous reactions.

513   Therefore, the significant growth of NH_3 in the morning determined the increase in nitrate, sulfate

514   and ammonium as well as that of aerosol hygroscopicity, which as a positive feedback retards the

515   decrease in atmospheric liquid water content and further enhances the hydrolysis of NO_2 as well

516   as the nitrate and sulfate formation.

517   Results in this paper reveals that the NH_3-promoted NO_2 hydrolysis is a significant source

518   of HONO, which provides direct insight into the missing daytime source of HONO on the NCP.

519   Results in this paper also shed light on the recent controversy of how SO_2, pH and NH_3 are involved

520   in heterogeneous HONO production. It was clarified that in the HONO production, SO_2 took a

521   minor part during fog events and an insignificant part during haze events, the observed growth in

522   sulfate was dominantly the byproduct of the HONO photolysis, confirming again the importance

523   HONO as an OH source and its crucial role in atmospheric chemistry.

524   These results have demonstrated the critical role and contribution of NH_3 in the formation

525   of photochemical and aerosol pollution on the North China Plain. Effective control measures are

526   urgently called for to reduce NH_3 emissions, which would simultaneously benefit the

527   photochemical and aerosol pollution abatement through the reduction of HONO production.

528 **Acknowledgments, Samples, and Data**

529   This work is supported by the National Key R&D Program of China (2016YFC0202300),
530 the National research program for key issues in air pollution control (DQGG0103) and the National
531 Natural Science Foundation of China (41505107 and 41590872). We thank Wei Peng from Beijing
532 Met High-Tech Co., Ltd. for his help with the maintenance of the IGAC instrument.

533

534 **Author contributions.** WX designed the experiment and YK led the research. YK, JT, GZ, YB,
535 YY, CS and LL were responsible for the aerosol measurements in the experiment, WY helped
536 with the IGAC measurements. WX made the trace gas measurements with the help of ZG, WL
537 and XX. WX and YK analyzed the data and wrote the paper.

538

539 **Competing interests**. The authors declare that they have no conflictof interest

540

541 **Data availability**. The data used in this study are available from the corresponding author upon
542 request (kuangye@jnu.edu.cn)

543

References

Cheng, Y., Zheng, G., Wei, C., Mu, Q., Zheng, B., Wang, Z., Gao, M., Zhang, Q., He, K., Carmichael, G., Pöschl, U., and Su, H.: Reactive nitrogen chemistry in aerosol water as a source of sulfate during haze events in China, Science Advances, 2, e1601530, 10.1126/sciadv.1601530, 2016.

Cui, L., Li, R., Zhang, Y., Meng, Y., Fu, H., and Chen, J.: An observational study of nitrous acid (HONO) in Shanghai, China: The aerosol impact on HONO formation during the haze episodes, The Science of the total environment, 630, 1057-1070, 10.1016/j.scitotenv.2018.02.063, 2018.

Ding, J., Zhao, P., Su, J., Dong, Q., and Du, X.: Aerosol pH and its influencing factors in Beijing, Atmos. Chem. Phys. Discuss., 2018, 1-34, 10.5194/acp-2018-270, 2018.

Guo, H., Weber, R. J., and Nenes, A.: High levels of ammonia do not raise fine particle pH sufficiently to yield nitrogen oxide-dominated sulfate production, Scientific reports, 7, 12109, 10.1038/s41598-017-11704-0, 2017.

Huang, R.-J., Yang, L., Cao, J., Wang, Q., Tie, X., Ho, K.-F., Shen, Z., Zhang, R., Li, G., Zhu, C., Zhang, N., Dai, W., Zhou, J., Liu, S., Chen, Y., Chen, J., and O'Dowd, C. D.: Concentration and sources of atmospheric nitrous acid (HONO) at an urban site in Western China, Science of The Total Environment, 593-594, 165-172, https://doi.org/10.1016/j.scitotenv.2017.02.166, 2017.

Kleffmann, J., Gavriloaiei, T., Hofzumahaus, A., Holland, F., Koppmann, R., Rupp, L., Schlosser, E., Siese, M., and Wahner, A.: Daytime formation of nitrous acid: A major source of OH radicals in a forest, Geophysical Research Letters, 32, doi:10.1029/2005GL022524, 2005.

Kuang, Y., Zhao, C. S., Tao, J. C., and Ma, N.: Diurnal variations of aerosol optical properties in the North China Plain and their influences on the estimates of direct aerosol radiative forcing, Atmos. Chem. Phys. Discuss., 15, 339-369, 10.5194/acpd-15-339-2015, 2015.

Kuang, Y., Zhao, C., Tao, J., Bian, Y., Ma, N., and Zhao, G.: A novel method for deriving the aerosol hygroscopicity parameter based only on measurements from a humidified nephelometer system, Atmos. Chem. Phys., 17, 6651-6662, 10.5194/acp-17-6651-2017, 2017.

Kuang, Y., Zhao, C. S., Zhao, G., Tao, J. C., Xu, W., Ma, N., and Bian, Y. X.: A novel method for calculating ambient aerosol liquid water content based on measurements of a humidified nephelometer system, Atmospheric Measurement Techniques, 11, 2967-2982, 10.5194/amt-11-2967-2018, 2018.

Li, L., Duan, Z., Li, H., Zhu, C., Henkelman, G., Francisco, J. S., and Zeng, X. C.: Formation of HONO from the NH3-promoted hydrolysis of NO2-dimers in the atmosphere, Proceedings of the National Academy of Sciences, 10.1073/pnas.1807719115, 2018a.

Li, L., Hoffmann, M. R., and Colussi, A. J.: Role of Nitrogen Dioxide in the Production of Sulfate during Chinese Haze-Aerosol Episodes, Environmental Science & Technology, 52, 2686-2693, 10.1021/acs.est.7b05222, 2018b.

Li, X., Brauers, T., Häseler, R., Bohn, B., Fuchs, H., Hofzumahaus, A., Holland, F., Lou, S., Lu, K. D., Rohrer, F., Hu, M., Zeng, L. M., Zhang, Y. H., Garland, R. M., Su, H., Nowak, A., Wiedensohler, A., Takegawa, N., Shao, M., and Wahner, A.: Exploring the atmospheric chemistry of nitrous acid (HONO) at a rural site in Southern China, Atmospheric Chemistry and Physics, 12, 1497-1513, 10.5194/acp-12-1497-2012, 2012.

Liu, M., Song, Y., Zhou, T., Xu, Z., Yan, C., Zheng, M., Wu, Z., Hu, M., Wu, Y., and Zhu, T.: Fine particle pH during severe haze episodes in northern China, Geophysical Research Letters, 44, 5213-5221, doi:10.1002/2017GL073210, 2017a.

Liu, Y., Wu, Z., Wang, Y., Xiao, Y., Gu, F., Zheng, J., Tan, T., Shang, D., Wu, Y., Zeng, L., Hu, M., Bateman, A. P., and Martin, S. T.: Submicrometer Particles Are in the Liquid State during

Heavy Haze Episodes in the Urban Atmosphere of Beijing, China, Environmental Science & Technology Letters, 4, 427-432, 10.1021/acs.estlett.7b00352, 2017b.

Liu, Z., Wang, Y., Costabile, F., Amoroso, A., Zhao, C., Huey, L. G., Stickel, R., Liao, J., and Zhu, T.: Evidence of Aerosols as a Media for Rapid Daytime HONO Production over China, Environmental Science & Technology, 48, 14386-14391, 10.1021/es504163z, 2014.

Lu, C., Niu, S., Tang, L., Lv, J., Zhao, L., and Zhu, B.: Chemical composition of fog water in Nanjing area of China and its related fog microphysics, Atmospheric Research, 97, 47-69, http://dx.doi.org/10.1016/j.atmosres.2010.03.007, 2010.

Lu, K., Guo, S., Tan, Z., Wang, H., Shang, D., Liu, Y., Li, X., Wu, Z., Hu, M., and Zhang, Y.: Exploring atmospheric free-radical chemistry in China: the self-cleansing capacity and the formation of secondary air pollution, National Science Review, nwy073-nwy073, 10.1093/nsr/nwy073, 2018.

Meng, Z., Xu, X., Lin, W., Ge, B., Xie, Y., Song, B., Jia, S., Zhang, R., Peng, W., Wang, Y., Cheng, H., Yang, W., and Zhao, H.: Role of ambient ammonia in particulate ammonium formation at a rural site in the North China Plain, Atmos. Chem. Phys., 18, 167-184, 10.5194/acp-18-167-2018, 2018.

Michoud, V., Colomb, A., Borbon, A., Miet, K., Beekmann, M., Camredon, M., Aumont, B., Perrier, S., Zapf, P., Siour, G., Ait-Helal, W., Afif, C., Kukui, A., Furger, M., Dupont, J. C., Haeffelin, M., and Doussin, J. F.: Study of the unknown HONO daytime source at a European suburban site during the MEGAPOLI summer and winter field campaigns, Atmos. Chem. Phys., 14, 2805-2822, 10.5194/acp-14-2805-2014, 2014.

Nie, W., Ding, A. J., Xie, Y. N., Xu, Z., Mao, H., Kerminen, V. M., Zheng, L. F., Qi, X. M., Huang, X., Yang, X. Q., Sun, J. N., Herrmann, E., Petäjä, T., Kulmala, M., and Fu, C. B.: Influence of biomass burning plumes on HONO chemistry in eastern China, Atmos. Chem. Phys., 15, 1147-1159, 10.5194/acp-15-1147-2015, 2015.

Petters, M. D., and Kreidenweis, S. M.: A single parameter representation of hygroscopic growth and cloud condensation nucleus activity, Atmospheric Chemistry and Physics, 7, 1961-1971, 2007.

Ran, L., Zhao, C. S., Xu, W. Y., Lu, X. Q., Han, M., Lin, W. L., Yan, P., Xu, X. B., Deng, Z. Z., Ma, N., Liu, P. F., Yu, J., Liang, W. D., and Chen, L. L.: VOC reactivity and its effect on ozone production during the HaChi summer campaign, Atmos. Chem. Phys., 11, 4657-4667, 10.5194/acp-11-4657-2011, 2011.

Safai, P. D., Kewat, S., Pandithurai, G., Praveen, P. S., Ali, K., Tiwari, S., Rao, P. S. P., Budhawant, K. B., Saha, S. K., and Devara, P. C. S.: Aerosol characteristics during winter fog at Agra, North India, J. Atmos. Chem., 61, 101-118, 10.1007/s10874-009-9127-4, 2008.

Shen, C., Zhao, C., Ma, N., Tao, J., Zhao, G., Yu, Y., and Kuang, Y.: Method to Estimate Water Vapor Supersaturation in the Ambient Activation Process Using Aerosol and Droplet Measurement Data, Journal of Geophysical Research: Atmospheres, 123, 10606-10619, doi:10.1029/2018JD028315, 2018.

Song, S., Gao, M., Xu, W., Shao, J., Shi, G., Wang, S., Wang, Y., Sun, Y., and McElroy, M. B.: Fine-particle pH for Beijing winter haze as inferred from different thermodynamic equilibrium models, Atmos. Chem. Phys., 18, 7423-7438, 10.5194/acp-18-7423-2018, 2018.

Stutz, J., Alicke, B., and Neftel, A.: Nitrous acid formation in the urban atmosphere: Gradient measurements of NO2 and HONO over grass in Milan, Italy, Journal of Geophysical Research: Atmospheres, 107, LOP 5-1-LOP 5-15, doi:10.1029/2001JD000390, 2002.

Su, H., Cheng, Y., Oswald, R., Behrendt, T., Trebs, I., Meixner, F. X., Andreae, M. O., Cheng, P., Zhang, Y., and Pöschl, U.: Soil Nitrite as a Source of Atmospheric HONO and OH Radicals, Science, 333, 1616-1618, 10.1126/science.1207687, 2011.

Teng, X., Hu, Q., Zhang, L., Qi, J., Shi, J., Xie, H., Gao, H., and Yao, X.: Identification of Major Sources of Atmospheric NH3 in an Urban Environment in Northern China During Wintertime, Environmental Science & Technology, 51, 6839-6848, 10.1021/acs.est.7b00328, 2017.

Vogel, B., Vogel, H., Kleffmann, J., and Kurtenbach, R.: Measured and simulated vertical profiles of nitrous acid—Part II. Model simulations and indications for a photolytic source, Atmospheric Environment, 37, 2957-2966, https://doi.org/10.1016/S1352-2310(03)00243-7, 2003.

Wang, G., Zhang, R., Gomez, M. E., Yang, L., Levy Zamora, M., Hu, M., Lin, Y., Peng, J., Guo, S., Meng, J., Li, J., Cheng, C., Hu, T., Ren, Y., Wang, Y., Gao, J., Cao, J., An, Z., Zhou, W., Li, G., Wang, J., Tian, P., Marrero-Ortiz, W., Secrest, J., Du, Z., Zheng, J., Shang, D., Zeng, L., Shao, M., Wang, W., Huang, Y., Wang, Y., Zhu, Y., Li, Y., Hu, J., Pan, B., Cai, L., Cheng, Y., Ji, Y., Zhang, F., Rosenfeld, D., Liss, P. S., Duce, R. A., Kolb, C. E., and Molina, M. J.: Persistent sulfate formation from London Fog to Chinese haze, Proceedings of the National Academy of Sciences, 10.1073/pnas.1616540113, 2016.

Whalley, L. K., Stone, D., George, I. J., Mertes, S., van Pinxteren, D., Tilgner, A., Herrmann, H., Evans, M. J., and Heard, D. E.: The influence of clouds on radical concentrations: observations and modelling studies of HO_x during the Hill Cap Cloud Thuringia (HCCT) campaign in 2010, Atmos. Chem. Phys., 15, 3289-3301, 10.5194/acp-15-3289-2015, 2015.

Wu, Z., Wang, Y., Tan, T., Zhu, Y., Li, M., Shang, D., Wang, H., Lu, K., Guo, S., Zeng, L., and Zhang, Y.: Aerosol Liquid Water Driven by Anthropogenic Inorganic Salts: Implying Its Key Role in Haze Formation over the North China Plain, Environmental Science & Technology Letters, 10.1021/acs.estlett.8b00021, 2018.

Xing, J., Ding, D., Wang, S., Zhao, B., Jang, C., Wu, W., Zhang, F., Zhu, Y., and Hao, J.: Quantification of the enhanced effectiveness of NOx control from simultaneous reductions of VOC and NH3 for reducing air pollution in the Beijing–Tianjin–Hebei region, China, Atmos. Chem. Phys., 18, 7799-7814, 10.5194/acp-18-7799-2018, 2018.

Xu, W. Y., Zhao, C. S., Ran, L., Lin, W. L., Yan, P., and Xu, X. B.: SO2 noontime-peak phenomenon in the North China Plain, Atmospheric Chemistry and Physics, 14, 7757-7768, 10.5194/acp-14-7757-2014, 2014.

Xue, L. K., Wang, T., Gao, J., Ding, A. J., Zhou, X. H., Blake, D. R., Wang, X. F., Saunders, S. M., Fan, S. J., Zuo, H. C., Zhang, Q. Z., and Wang, W. X.: Ground-level ozone in four Chinese cities: precursors, regional transport and heterogeneous processes, Atmos. Chem. Phys., 14, 13175-13188, 10.5194/acp-14-13175-2014, 2014.

Yabushita, A., Enami, S., Sakamoto, Y., Kawasaki, M., Hoffmann, M. R., and Colussi, A. J.: Anion-Catalyzed Dissolution of NO2 on Aqueous Microdroplets, The Journal of Physical Chemistry A, 113, 4844-4848, 10.1021/jp900685f, 2009.

Ye, C., Liu, P., Ma, Z., Xue, C., Zhang, C., Zhang, Y., Liu, J., Liu, C., Sun, X., and Mu, Y.: High H2O2 Concentrations Observed during Haze Periods during the Winter in Beijing: Importance of H2O2 Oxidation in Sulfate Formation, Environmental Science & Technology Letters, 10.1021/acs.estlett.8b00579, 2018.

Yin, Z., Ye, X., Jiang, S., Tao, Y., Shi, Y., Yang, X., and Chen, J.: Size-resolved effective density of urban aerosols in Shanghai, Atmospheric Environment, 100, 133-140, http://dx.doi.org/10.1016/j.atmosenv.2014.10.055, 2015.

679   Young, L.-H., Li, C.-H., Lin, M.-Y., Hwang, B.-F., Hsu, H.-T., Chen, Y.-C., Jung, C.-R., Chen,
680   K.-C., Cheng, D.-H., Wang, V.-S., Chiang, H.-C., and Tsai, P.-J.: Field performance of a semi-
681   continuous monitor for ambient PM2.5 water-soluble inorganic ions and gases at a suburban site,
682   Atmospheric Environment, 144, 376-388, https://doi.org/10.1016/j.atmosenv.2016.08.062, 2016.
683   Zheng, G. J., Duan, F. K., Su, H., Ma, Y. L., Cheng, Y., Zheng, B., Zhang, Q., Huang, T., Kimoto,
684   T., Chang, D., Pöschl, U., Cheng, Y. F., and He, K. B.: Exploring the severe winter haze in Beijing:
685   the impact of synoptic weather, regional transport and heterogeneous reactions, Atmos. Chem.
686   Phys., 15, 2969-2983, 10.5194/acp-15-2969-2015, 2015.

687

688

689

690
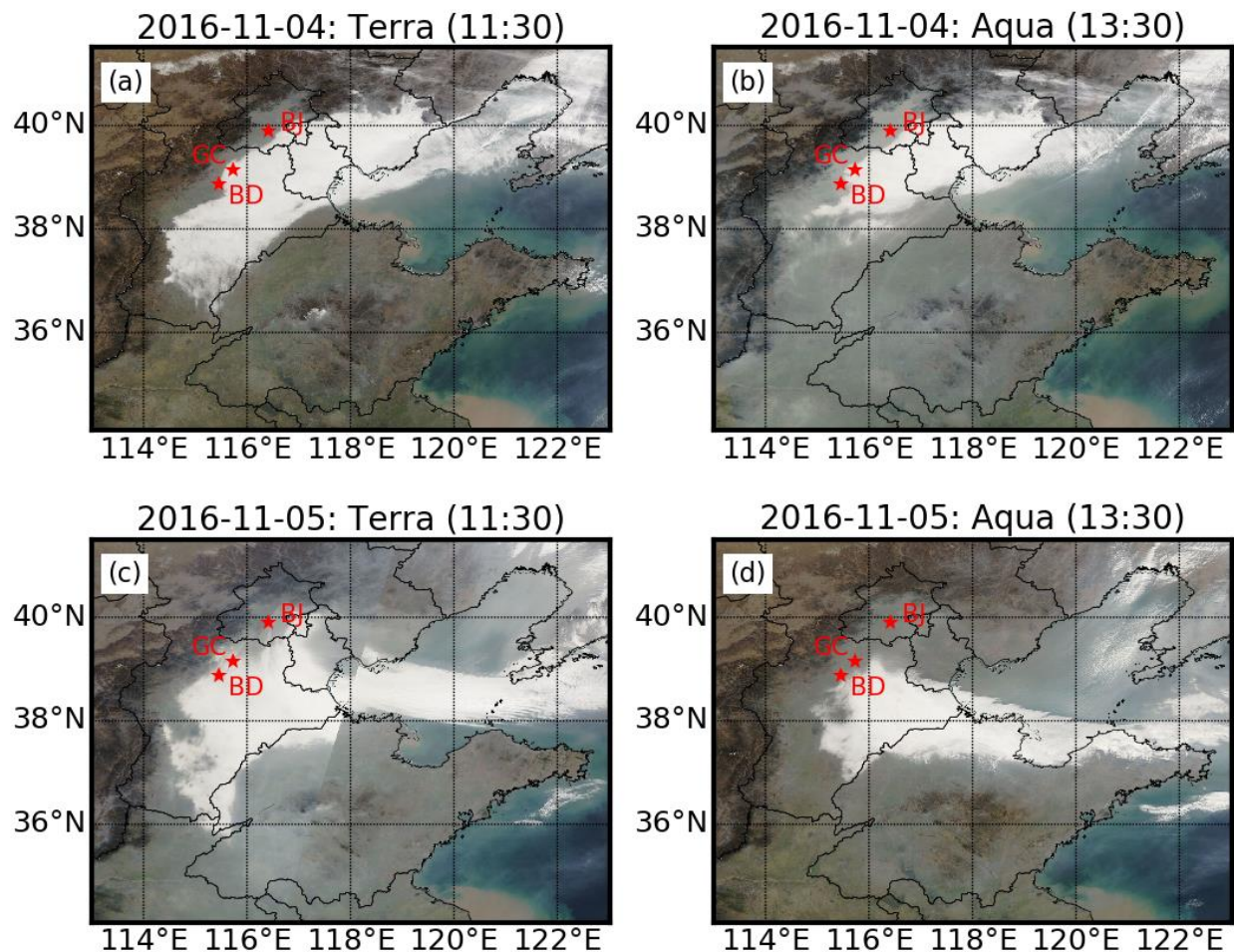
691
Figure 1. MODIS Terra (a,c) and Aqua (b,d) satellite images in 04th Nov. (a,b) and 5th Nov. 2016
(c,d), star markers are locations of Gucheng (GC: the observation site), Baoding (BD) and Beijing
(BJ).
695

696
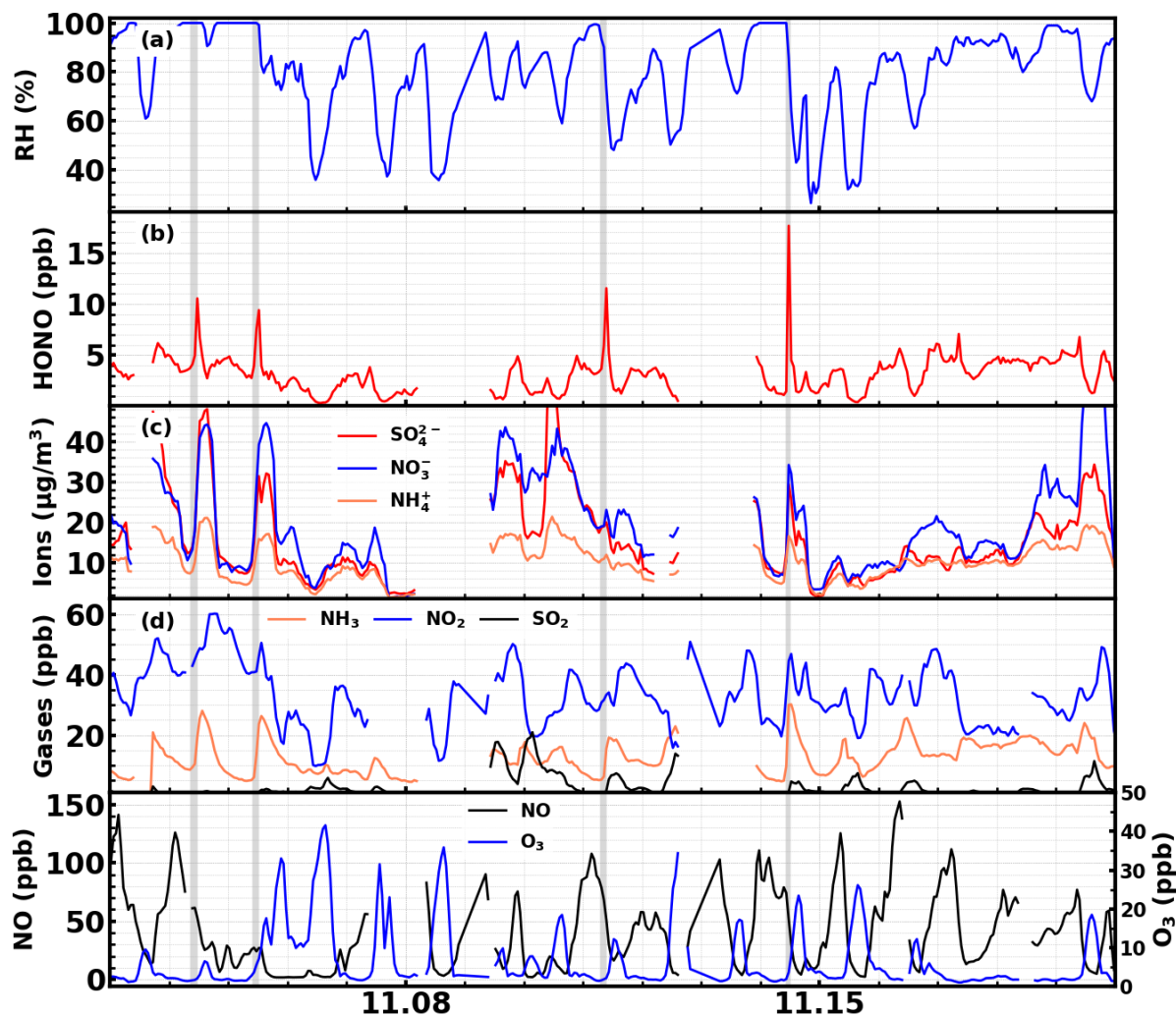
697 **Figure 2**. Time series of ambient **a)** RH; **b)** HONO; **c)** sulfate, nitrate, ammonium; **d)** NH_3, NO_3
698 and SO_2 during the observation period.

699
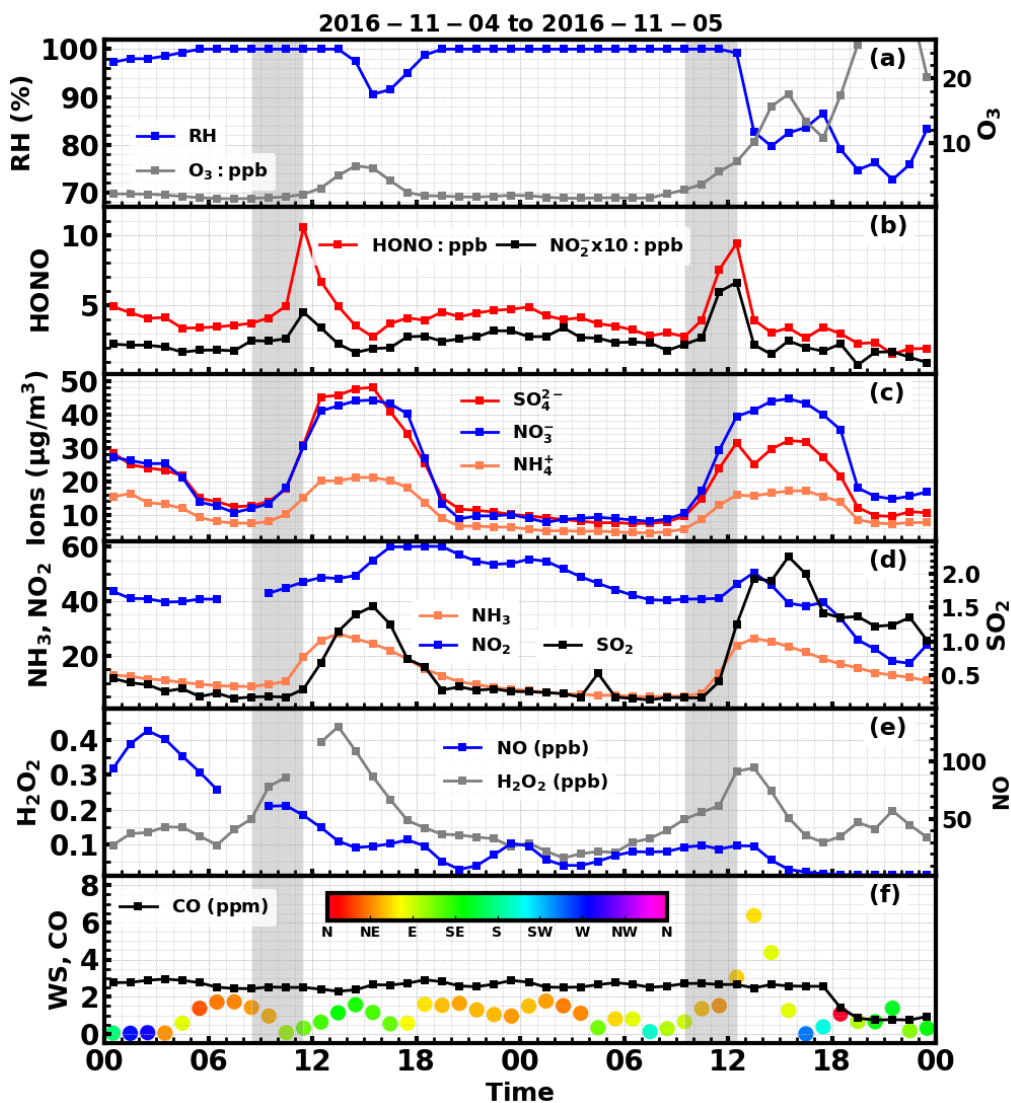
700
Figure 3. Time series of ambient **a)** RH,O_3, **b)**HONO, NO_2^-, **c)** SO_4^{2-}, NO_3^-, NH_4^+, **d)** NH_3, NO_2,
SO₂, **e)** NO, H₂O₂, **f)** CO, wind speed and wind direction (colors of scatter points) from 4th to 5th
Nov. 2016. Gray shaded areas represent periods of rapid increase of HONO.
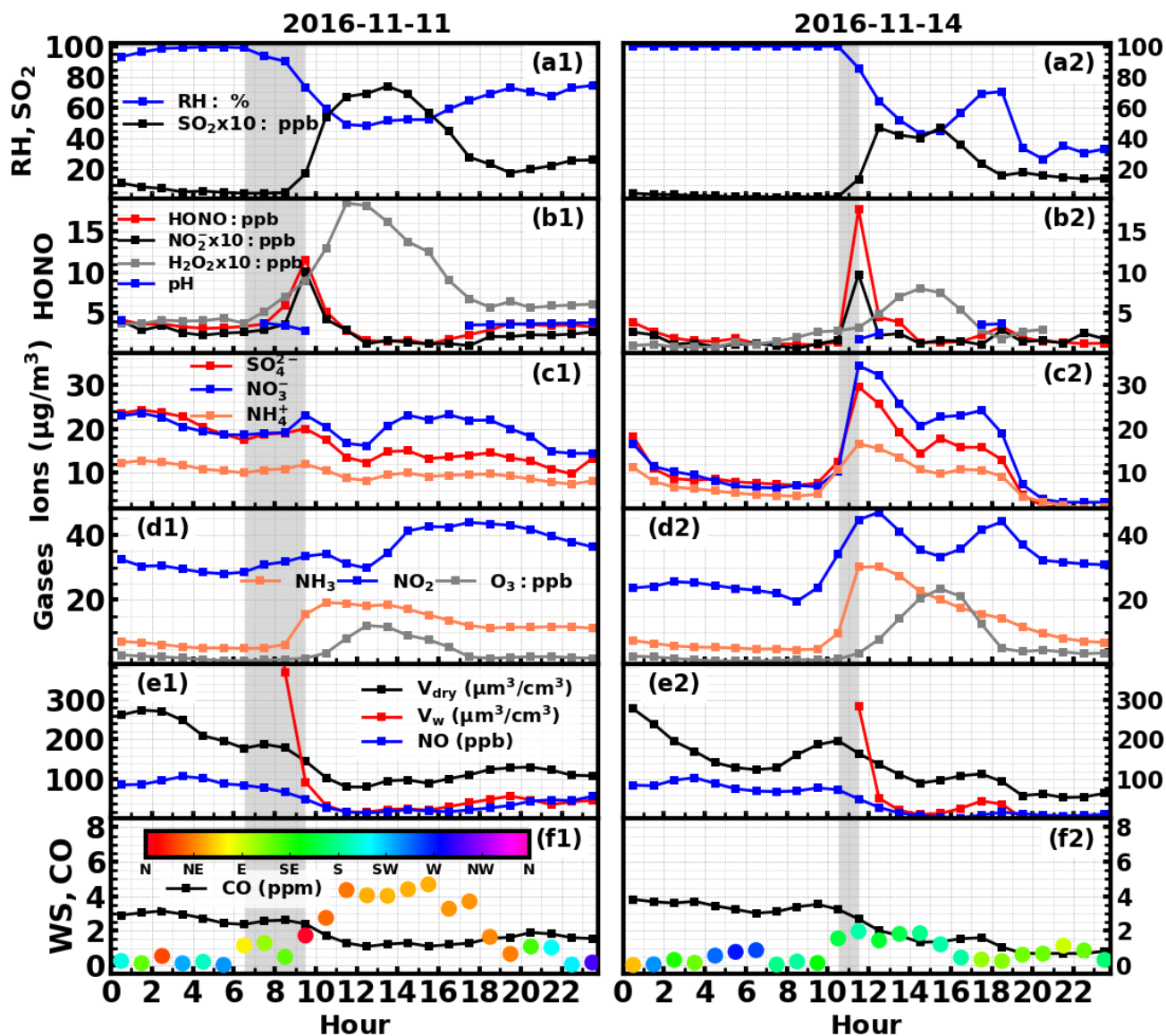
704
705 **Figure 4**. Time series of ambient **a)** RH, SO₂, **b)** HONO, NO₂⁻, H₂O₂, aerosol pH, **c)** SO_4^{2-}, NO_3^-,
706 NH_4^+, **d)** NH₃, NO₂, O₃, **e)** NO, volume concentrations of PM₂.₅ in dry state (V_{dry}), volume
707 concentrations of liquid water (V_w), **f)** CO, wind speed and wind direction during **1)** 11th Nov. 2016
708 and **2)** 14th Nov. 2016. Gray shaded areas represents periods of rapid increase of HONO.

709
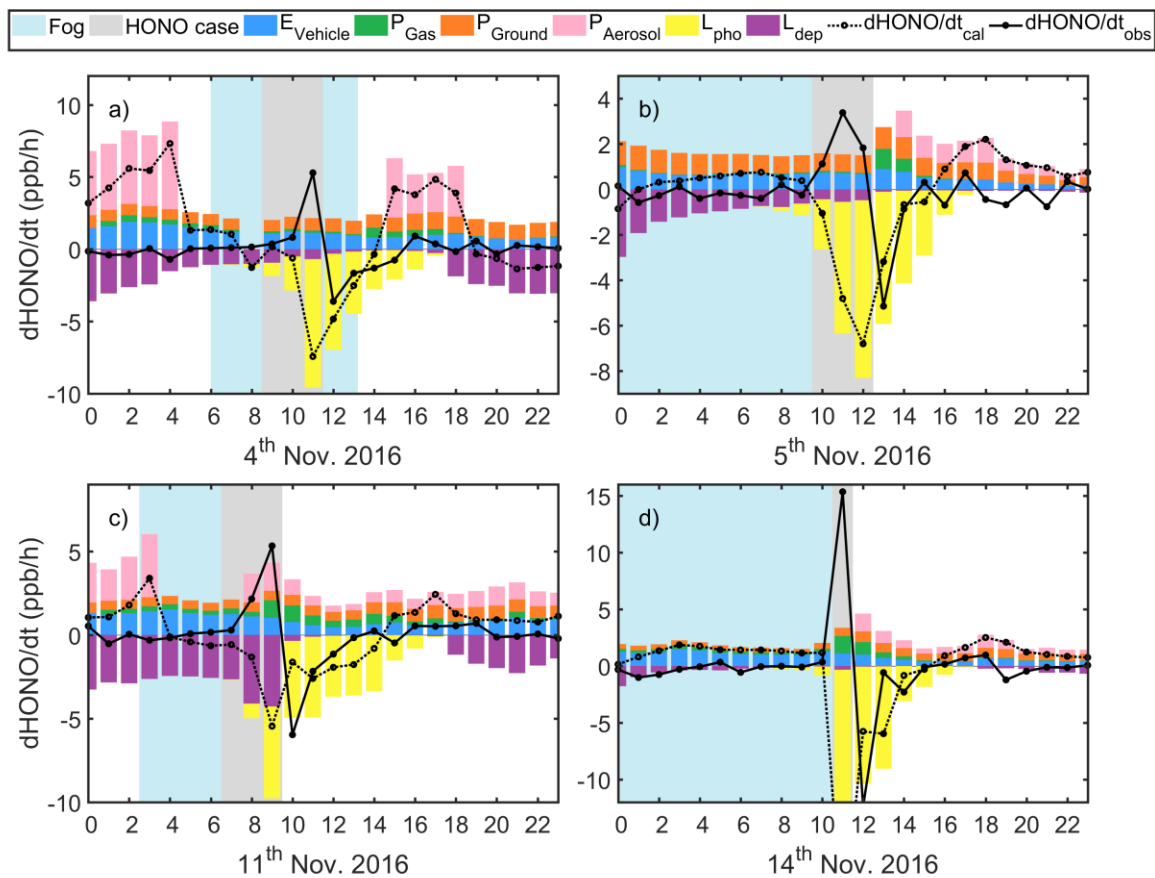
Figure 5. Estimated HONO emission from vehicles (blue), gas phase production (green), production on ground (orange) and aerosol surface (pink), loss through photolysis (yellow) and dry deposition (purple), as well as the calculated (dotted black) and actually observed (solid black) d[HONO]/dt on a) 4th, b) 5th, c) 11th and d) 14th Nov. 2016
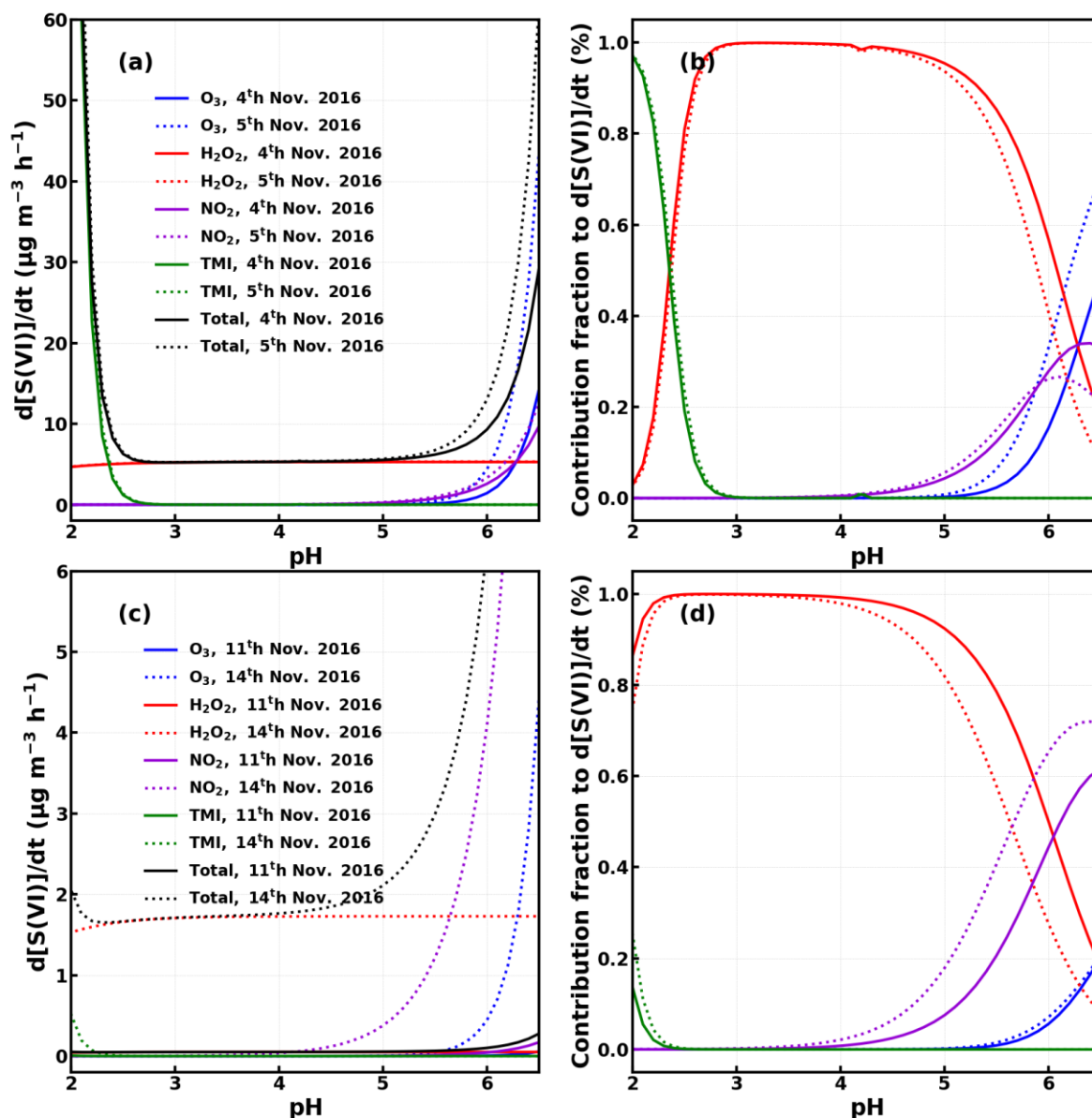
714
715 **Figure 6.** Calculated average sulfate production (a,c) and contribution fraction b,d) from SO_2
716 oxidation by H_2O_2, NO_2, O_3, TMI under different pH values using methods described in (Cheng et
717 al., 2016) for the case episodes on 4th, 5th, 11th and 14th Nov. 2016.
718
719
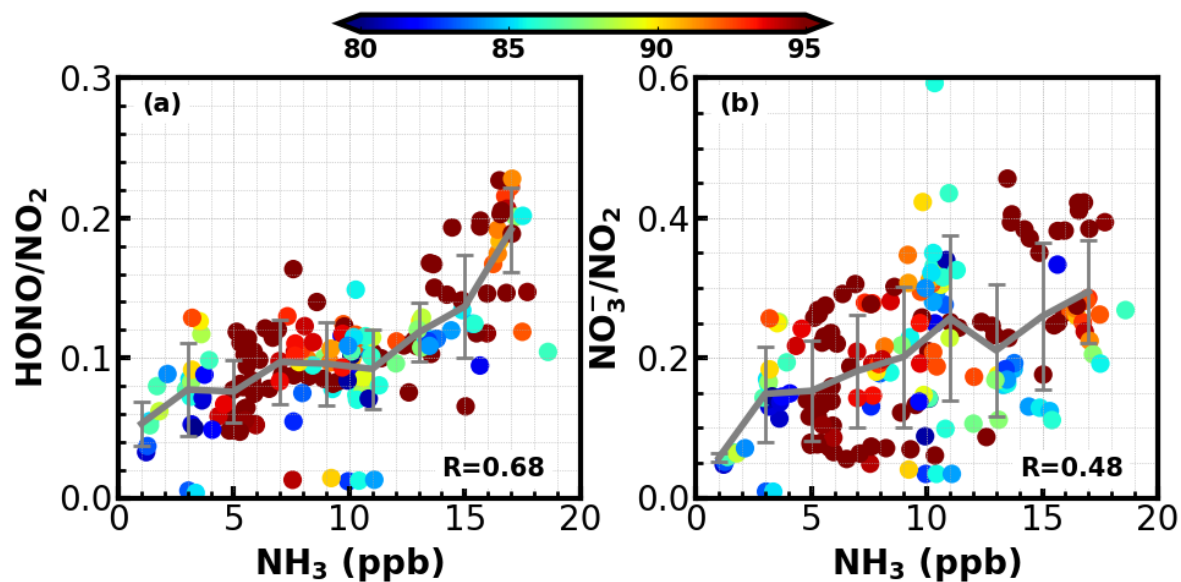
720
721 **Figure 7**. The relationship between NH$_3$ concentration and **a)** HONO/NO$_2$ ratio; **b)**
722 nitrate/nitrogen dioxide ratio (NO_3^-/NO_2); Colors of scatter points represent ambient RHs and the
723 color bar is shown on the top.
724
725
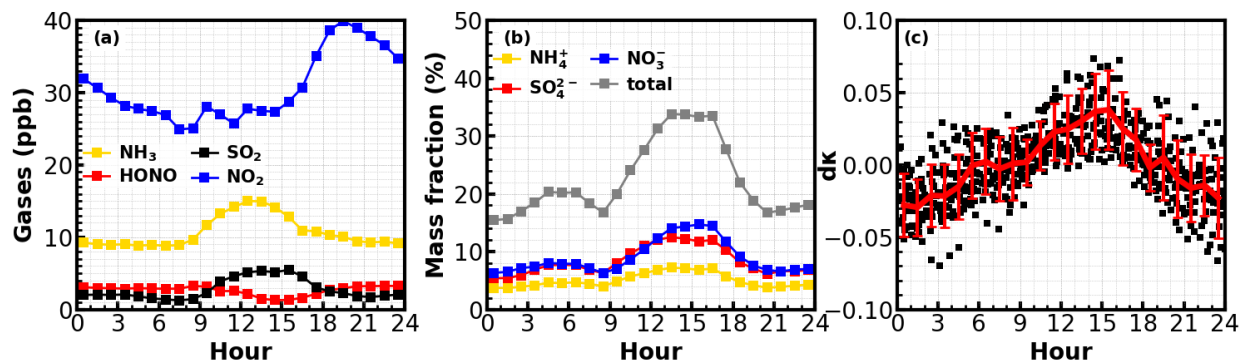
726
727 **Figure 8.** **(a)** Average diurnal variations of Gases; **(b)** Average diurnal variations mass fractions
728 of nitrate, sulfate and ammonium; **(c)** Diurnal variations of aerosol hygroscopicity, dκ is the
729 anomaly to the daily mean κ.